685

26 January 1981

Letter of Intent

An investigation of the behaviour of the photon in deep inelastic photon hadron collisions

Bari - Fermilab - Max-Planck-Institut Munich

Collaboration

Spokesman:
K.P. Pretzl
MPI Munich

Contactman:
W. Baker
Fermilab

1.) Introduction

As a continuation of our present research program at the SPS at CERN where we investigate deep inelastic scattering processes involving photons in either the initial or the final state we intend to profit from the high intensity and high energy photon beams available from the Tevatron at Fermilab to study the behaviour of the photon in deep inelastic photon hadron scattering.

In particular we propose to search for any deviation from the hadron like behaviour of the photon by comparing photon-hadron with hadron-hadron collisions. We will look for evidence of the point like nature of the photon, which would manifest itself in events where the total energy of the incident photon is observed at large angles in a large acceptance calorimeter. The detection of such deep inelastic scattering processes would be a valuable test of QCD.

The apparatus is schematically sketched in Fig. 1 and consists of the two calorimeters used in the NA-5 experiment at CERN, a fast proportional chamber telescope, a liquid hydrogen target and a tagging system for the incident photons. It is the intention to perform the experiment in the new wide-band neutral beam for the Tevatron as proposed by J. Butler et al. [1]. The calorimeters and the large size modules of the proportional chambers will be shipped from CERN to Fermilab.

2.) Motivation

Because of its three component nature the photon is a particularly interesting particle to be studied. In most photon-hadron collisions the photon behaves like a vector meson (vector dominance behaviour VMD). However in some rare cases the photon is expected to interact point like with partons. These hard scattering processes are shown in fig. 2a,b,c, and have been discussed in a number of theoretical papers [2-9]. They have the characteristic feature that the incident photon transmits all its energy to the outgoing partons, which should be observable as jets in the final state. Except for the QED-Compton process, where one of the outgoing partons is replaced by a photon, 3 jet events with two large p_T jets and one target spectator jet are expected. Deep inelastic scattering events of this type can be selected from the ordinary vector meson like events by requiring that all of the incident photon energy is carried off at large angles with respect to the incident beam direction. They should be found at $x_c = 1$ where x_c is the fraction of the incident beam energy measured at large angles in the calorimeter. Also one could require that the transverse energy $\Sigma|p_T|$ of all particles in the final state is large.

Deviations from VMD are also expected in the region below $x_c = 1$. These reactions where the photon first hadronises ("hard" component of the photon) and then interacts with the target are discussed by Tu Tung-sheng [5]. As shown in fig. 3 they lead to 4 jets in the final state consisting of two large p_T jets and two beam/target spectator jets. These events are interesting in their own right.

The cross sections $\frac{d\sigma}{dx_c}$ for the 3 jet, 4 jet and VMD reactions were calculated assuming pencil like jets for the calorimeter acceptance of 30^o to 110^o in cms polar angle Θ^*, and 2π in azimuthal angle under the assumptions described in the Appendix (see fig. 4). For kinematical reasons x_c is equal to the fractional momentum x of the interacting constituent in the incident particle for values $x_c > 0.5$.

In fig. 5 the percentage contributions of the 3 and 4 jet cross sections to the total high p_T jet-photo-production cross section are plotted as a function of $x_\perp = \frac{2p_T}{\sqrt{s}}$. As can be seen in figs 4 and 5 the point like interaction of the photon dominates at large $x_\perp$ and shows a pronounced peak at $x_c = 1$. The cross sections for QED-Compton scattering, which also peak at $x_c = 1$, are expected to be a factor α/α_s smaller than for QCD-Compton scattering.

As a result of the particular shape of the "hard" photon structure function, taken from Ref. [10]and shown in fig. 6, the 4 jet cross sections are rather flat in x_c. The "hard" and the "point like" component of the photon structure function both peak near $x_c = 1$. Therefore the distinction between 3 and 4 jet events is highly dependent on our ability to identify individual jets in this region.

The effects of the calorimeter resolution and the finite jet size have been studied in a Monte-Carlo-simulation and the resulting cross sections are shown in fig. 7. The assumed jet size and multiplicity distribution were basedon the e^+e^- data. The smearing of the QCD-Compton peak at $x_c = 1$ is due to the jet sizes and to the energy resolution of the calorimeter.

We point out that the comparison of pion and photon induced reactions should show directly any deviation from the hadron like behaviour of the photon. Even if the photon behaves like a pion at low values of x_c its "point like" interactions with partons should be detectable near to $x_c = 1$.

Recent results obtained with the PLUTO detector at PETRA [11,12] have shown evidence for a hard scattering component of the photon in the process $\gamma + \gamma \rightarrow$ jet + jet.

We propose to measure the cross sections

$\frac{d\sigma}{dx_c}$ and $\frac{d\sigma}{dx_\perp}$ with $x_\perp = \frac{\Sigma|p_T|}{\sqrt{s}}$ and $\Sigma|p_T|$ the transverse energy observed in the calorimeter for γp and $\pi^- p$ interactions at 200 and 350 GeV with the same detector and trigger requirements. To better understand the finite calorimeter acceptance we perform these measurements at various cms cut off angles.

The data will be investigated for:

(i) any deviation from a hadron like behaviour of the photon;

(ii) the QCD-Compton peak at $x_c = 1$. The cross sections will be compared to QCD-model predictions;

(iii) the energy dependence of the γp cross section at $x_c = 1$;

(iv) jets in the final state. If jets can be reconstructed we will investigate the scaling behaviour of the γp cross sections parameterised as:

$$E \frac{d^3\sigma}{dp^3} \sim p_T^{-n} \; f(x_\perp)$$

3.) Detector

The major items of the detector are the two calorimeters which have been used in the NA-5 experiment. For measuring the energy of secondary particles coming from an interaction in the target we choose to rely on the calorimeter. This solution has the following features:

a) there is a fully symmetric 2π acceptance for the $\Sigma|p_T|$-trigger;

b) the flux of e^+e^- pairs produced with incident photons on the target is confined to a region of a few centimeters around the incident beam axis;

c) the granular structure of the calorimeter enables a search for jets in the final state, which should manifest themselves as energy clusters observed in the photon-hadron calorimeter.

3.1. Track Detector

A track detector consisting of two groups of multiwire proportional chambers MWPC will be used to reconstruct the vertex.

The first group of MWPC consists of 4 modules with 2 wire planes each of 1x1 m^2 and wire spacing of 2 mm. The wires in the different planes will be inclined at some angle in order to eliminate ambiguities in the projected trajectories and reconstruct the space points. The second group consists of 3 large modules with 4 wire planes each 2x2 m^2. The wire spacing will be 3 mm and the wire inclination similar to that in the first group.

A background study of e^+e^- pairs produced in the target has shown that the e^+e^- flux is confined to a region of a few cm diameter around the incident beam axis. In this region the MWPC will be deadened by beam killers.

3.2. Calorimeters

The ring calorimeter, a barrel of 3 m diameter with a 56 cm central hole, has a lead-scintillator sandwich photon section (16 x 0.55 cm Pb-sheets) followed by an iron-scintillator sandwich hadronic section (20 x 5 cm Fe-sheets) (see fig. 8). Both sections are subdivided into 240 independent cells, each subtending about 9^o in the cms polar angle and 15^o in azimuthal angle. Combined wave length shifting acrylic rods (doped with Yellow 323 and BBQ) were used to draw separated signals from the photon and hadron part of the calorimeter onto 240 pairs of photomultiplier tubes. This novel light-collection system has been described in Ref. [13] and is schematically shown in fig. 9. The obtained energy resolutions were $\sigma/E = 0.23/\sqrt{E}$ for electrons and $\sigma/E = 0.71/\sqrt{E} + 0.06$ for hadrons. In fig. 10 the energy resolution of the hadron calorimeter is compared to the results from other hadron calorimeters (for Refs. see [13]).

The $\Sigma|p_T|$-trigger can be derived from the sum of the analogue signals of all or part of the calorimeter cells weighted by their radial distance from the beam axis. The shape of the trigger pulses will be recorded. Occasional background triggers due to Cerenkov light produced in the acrylic rods can be eliminated to a large extent off-line by pulse shape analysis.

The downstream calorimeter, which covers the central hole of the ring calorimeter, will measure the energy flow at small angles. It is 1 x 1 m^2 in cross section and contains a photon and a hadron section each subdivided into 4 independent cells with a beam hole of 6 cm diameter in the center. The photon section consists of 16 x 0.55 cm Pb sheets sandwiched with Plexipop scintillator sheets of 2.5 cm thickness. The hadron section contains 25 x 5 cm Fe sheets sandwiched with scintillator sheets of 2.5 cm thickness. The scintillator light of each cell is collected by an acrylic bar doped with BBQ wavelength shifter material and guided onto a photomultiplier (see fig. 11). The measured energy resolution for hadrons is $\sigma/E = 7\%$ at 340 GeV/c and $\sigma/E = 11\%$ at 80 GeV/c, while for photons the resolution is $\sigma/E = 2\%$ at 80 GeV/c.

Both the ring and the downstream calorimeters are mounted on rails and can be moved along, and to some extent also perpendicular to the beam axis.

4.) Beam

Our Monte-Carlo studies have shown that the distinction of the 3 and 4 jet events depends strongly on the jet size and improves with increasing incident photon energy. We therefore intend to perform the experiment in a beam which provides the highest possible photon energies and intensities.

Preliminary calculations of J. Butler et al. for a new wide-band neutral beam show that photon intensities of $4.5 \cdot 10^7$ and $1.5 \cdot 10^7$ for energies of $E\gamma > 200$ GeV and $E\gamma > 350$ GeV respectively are possible to obtain with $6 \cdot 10^{12}$ incident protons per Tevatron spill (fig. 12).

A tagging system with an energy resolution $\Delta E\gamma/E\gamma = \pm 5\%$ is required by this experiment. Small scintillator hodoscopes positioned in the incident electron beam and after the radiator will be used to measure the momenta of the electrons before and after Bremsstrahlung. Such a tagging system can handle the expected electron intensities of $3.6 \cdot 10^8$ electrons at 450 GeV per $6 \cdot 10^{12}$ incident protons within a Tevatron spill of 20 sec.

This beam is also able to transport high energy negative pions for the comparison of pion and photon induced reactions.

5.) Rates, Trigger, Background

Rates:

The estimated cross sections and events per day for the QCD processes $\gamma p \rightarrow 3$ jets at 350 GeV are listed in table 1. The following assumptions entered the calculations:

a) $1.5 \cdot 10^7$ tagged incident photons per Tevatron spill with $E\gamma > 350$ GeV derived from a 450 GeV electron beam. To obtain this intensity $6 \cdot 10^{12}$ incident protons are required at the production target.

b) 30 cm long liquid H_2-target

c) 1 Tevatron spill per minute

d) 50% overall efficiency in the data taking

e) a calorimeter acceptance of 30^{o} to 110^{o} in the cms polar angle Θ^*, and 2π in the azimuth. Pencil like jets were assumed and both large p_T jets were required to be within the acceptance of the calorimeter. A $p_T \geq 2$ GeV/c was required for each of the large p_T jets.

This gives a sensitivity of about 14 events/nb day.

Trigger:

Data will be taken with a minimum bias trigger requiring that the incident photon produces hadrons in the hydrogen target and a small fraction of the total incident energy $x_c > 0.3$ be observed in the ring calorimeter. With a $x_c > 0.3$ trigger requirement we would expect 17 events per Tevatron spill. With this data taking rate there is practically no dead time loss. All other triggers can be applied essentially off-line.

<u>Background for the Trigger</u>:

a) e^+e^- pairs produced in the hydrogen target are mostly confined to a small region around the beam axis. Possible background coming from these or from photons and electrons originating upstream of the target are rejected by the trigger by accepting only events which have a certain amount of energy deposited in the hadronic section of the calorimeter.

b) Halo particles possibly giving rise to large p_T triggers are vetoed by a large scintillation counter array positioned upstream of the H_2-target.

References

1. J. Butler et al., TM-963 6020.00 Fermilab report, Design for a new wide-band neutral beam for the Tevatron.
2. J.D. Bjorken and E.A. Paschos, Phys.Rev. D, 185, 5 (1969) 1975.
3. H. Fritsch and P. Minkowski, Phys.Lett. 69 B 3 (1977) 316.
4. W. Ochs and L.Stodolsky private communication.
5. Tu Tung-Sheng, Nucl. Phys. B 161 (1979) 417.
6. J.F. Owens, Phys. Rev. D, 21 (198o) 54.
7. Tu Tung-Sheng and Wu Chi-Min, Ref. TH 2646-CERN.
8. Chang-Chao-Hsi, Tu Tung-Sheng and Wu Chi-Min, Ref. TH 2675-CERN.
9. M. Fontannaz et al., Ref. LPTHE 80/12 A 393-0480.
10. C.H. Llewellyn Smith, Phys. Lett. 79 B (1978) 83, and I. Kang and C.H. Llewellyn Smith, preprint Oxford Univ.Ref.62/79.
11. W. Wagner "Two-photon results from PETRA" presented at the XXth International Conference on High Energy Physics at Madison 1980.
12. B. Wiik "New e^+e^- Physics" presented at the XXth International Conference on High Energy Physics at Madison 1980.
13. V. Eckardt, R. Kalbach, A. Manz, K. Pretzl, N. Schmitz and D. Vranic, Nucl. Inst. and Meth. 155 (1978) 389-398.
14. V. Barger and R. Phillips, Nucl. Phys. B73 (1974) 269.

Table 1

Estimated cross sections and event rates for the QCD processes $\gamma p \to 3$ jets. The assumptions are explained in the text.

$E\gamma = 350$ GeV

p_T of one jet [GeV/c]	$x_T = \frac{2p_T}{\sqrt{s}}$	$\frac{d\sigma}{dp_T}$ [nb/GeV/c]	$\frac{\text{events}}{\text{day}}$
3.5	0.27	14.8	204
4.5	0.35	43.6	602
5.5	0.43	31.2	430
6.5	0.51	12.9	178
7.5	0.58	4.64	64
8.5	0.66	1.45	20
9.5	0.74	0.42	6
10.5	0.82	0.087	1
11.5	0.90	0.0092	0.1
		$\sigma_{x_c=1} = 109$ nb	1504.2

Figure Captions

Fig. 1: Experimental layout

Fig. 2: First order Feynman graphs for QCD- and QED-Compton-scattering.

Fig. 3: Interactions where the photon hadronises before interacting (taken from Ref. 5).

Fig. 4: Cross sections for pencil-like jets produced in 350 GeV γp interactions, where x_c is the fraction of the laboratory energy detected by the calorimeter.

Fig. 5: Expected percentage contributions of the different "hard" interactions as a function of $x_{\perp} = \frac{2p_T}{\sqrt{s}}$ of a single pencil-like jet.

Fig. 6: The photon structure function F(x) in units of $\alpha \ln Q^2 \pi^{-1}$:

a) $xq(x)$ for charge 2/3 quarks
b) $xq(x)$ for charge 1/3 quarks
c) $xg(x)$ for gluons
d) $xq(x)$ for charge 2/3 quarks in the born approximation of Ref. 10.

Fig. 7: Differential cross sections $d\sigma/dx_c$ for the expected contributions to 350 GeV γp interactions, where jet fragmentation and calorimeter resolution have been taken into account for point like coupling (3 jets) and the hard component + VMD (4 jets). The cross sections are shown for two different calorimeter acceptances $30^\circ < \theta^* < 110^\circ$ and $45^\circ < \theta^* < 135^\circ$.

Fig. 8: The photon-hadron ring calorimeter used in the NA-5 experiment, showing segmentation into 10 rings and 24 sectors.

Fig. 9: Details of the construction and the light collection system used in the ring calorimeter.

Fig. 10: The energy resolution of the hadronic part of the ring calorimeter compared with previously published results.

Fig. 11: Constructional details of the downstream calorimeter.

Fig. 12: Expected photon intensities at the Tevatron (taken from Ref. 1).

APPENDIX

The following assumptions were made when estimating the cross sections for the QCD processes:

RUNNING COUPLING CONSTANT

$$\alpha_s = \frac{12\pi}{25 \log \frac{Q^2}{\Lambda^2}}, \quad \Lambda = 0.5, \quad Q^2 = \frac{2\,\hat{s}\,\hat{t}\,\hat{u}}{\hat{s}^2 + \hat{t}^2 + \hat{u}^2}$$

PROTON STRUCTURE FUNCTIONS from Barger, Phillips [14]

$$xu(x) = x^{1/2}[0.594\ (1-x^2)^3 + 0.461\ (1-x^2)^5 + 0.621\ (1-x^2)^7]$$

$$xd(x) = x^{1/2}[0.072\ (1-x^2)^3 + 0.206\ (1-x^2)^5 + 0.621\ (1-x^2)^7]$$

SEA DISTRIBUTION: $xs(x) = 0.145\ (1-x)^9$

GLUON DISTRIBUTION: $xg(x) = 3\ (1-x)^5$

PION STRUCTURE FUNCTIONS from the results of the NA3 experiment

$$xu(x) = xd(x) = 0.75\ \sqrt{x}(1-x)$$

SEA DISTRIBUTION $xs(x) = 0.145\ (1-x)^9$

GLUON DISTRIBUTION $xg(x) = 2\ (1-x)^3$

PHOTON STRUCTURE FUNCTIONS from [10]

1) QCD COMPONENT

a) CHARGE $\frac{2}{3}$

$$xu(x,Q^2) = x\bar{u} = xc = x\bar{c} = \frac{\alpha}{\pi}\ \ell n\ \frac{Q^2}{\Lambda^2}\ (0.077 + 0.175x)$$

b) CHARGE $\frac{1}{3}$

$$xd(x,Q^2) = x\bar{d} = xs = x\bar{s} = \frac{\alpha}{\pi}\ \ell n\ \frac{Q^2}{\Lambda^2}\ (0.027 + 0.033x)$$

2) HADRON LIKE PIECE (VMD)

$$u(x) = \bar{u} = 4d = 4\bar{d} = \left(\frac{e}{2\gamma_\rho}\right)^2 \frac{4}{9} f(x)$$

$$s(x) = \bar{s}(x) = \left(\frac{M_O}{M_\phi}\right)^2 d(x) \text{ (strange q)}$$

$$c(x) = \bar{c}(x) = \left(\frac{M_O}{M_\psi}\right)^2 u(x)$$

where $f(x) = u^\pi(x)$ and $\frac{\gamma_\rho^2}{4\pi}$ is ρ-meson-photon coupling constant

$\left(\frac{\gamma_\rho^2}{4\pi} = 0.54\right)$.

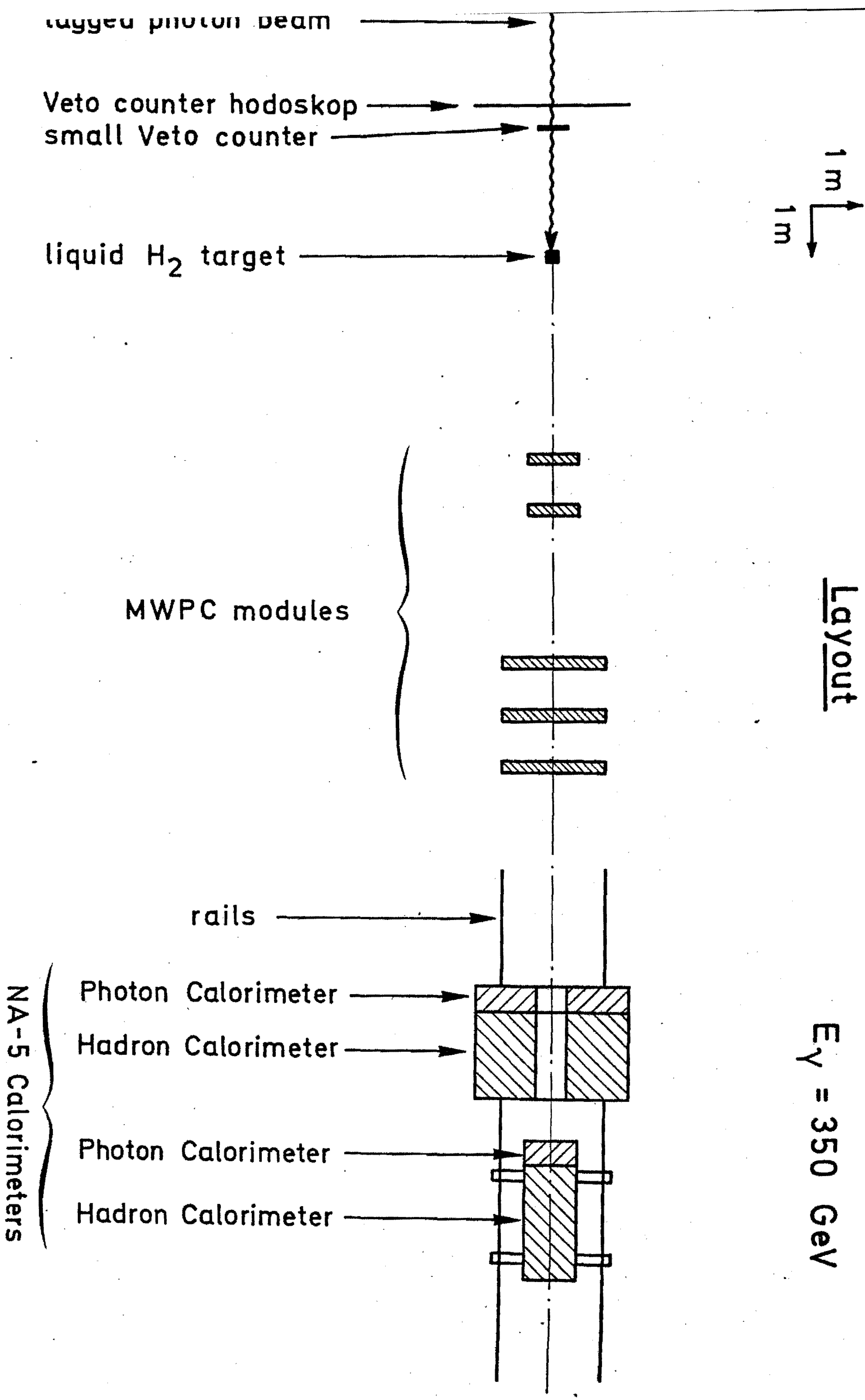
tagged photon beam
Veto counter hodoskop
small Veto counter
liquid H_2 target
1 m
1 m
MWPC modules
Layout
rails
Photon Calorimeter
Hadron Calorimeter
Photon Calorimeter
Hadron Calorimeter
NA-5 Calorimeters
E_γ = 350 GeV

Fig. 1

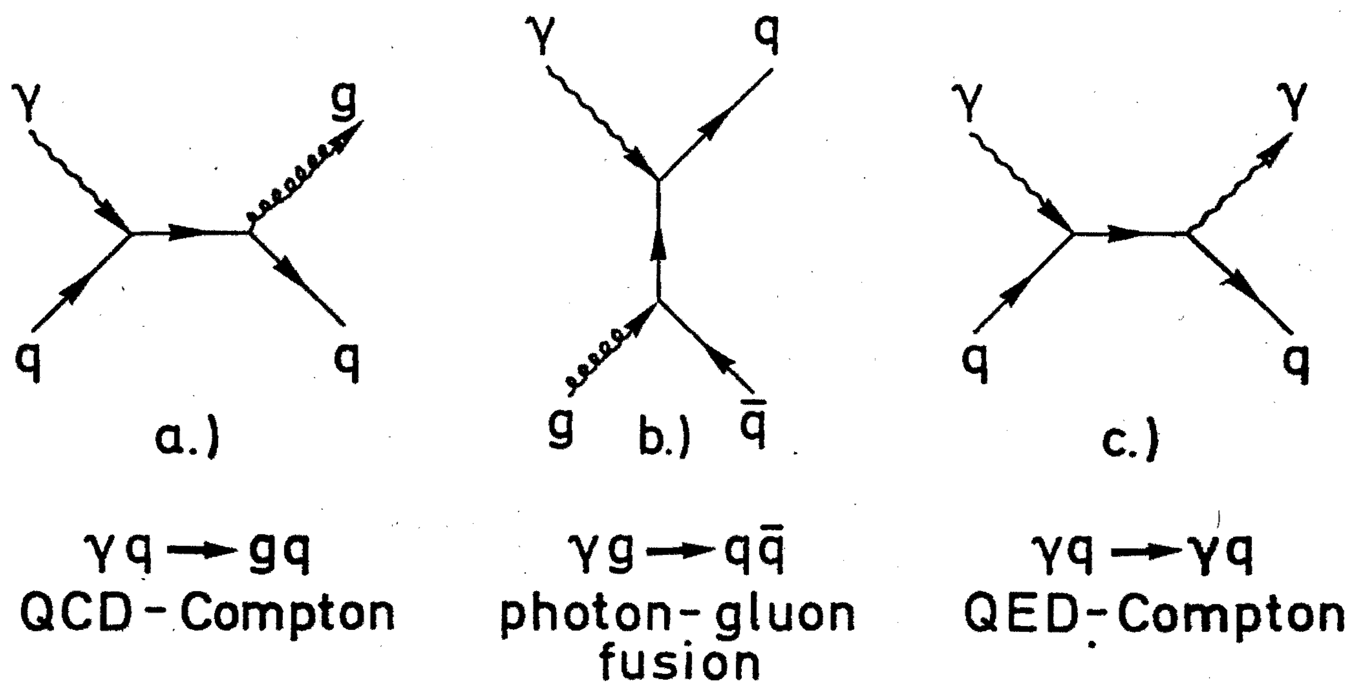
a.)
γq → gq
QCD - Compton
b.)
γg → q$\bar{q}$
photon - gluon fusion
c.)
γq → γq
QED - Compton

FIG. 2

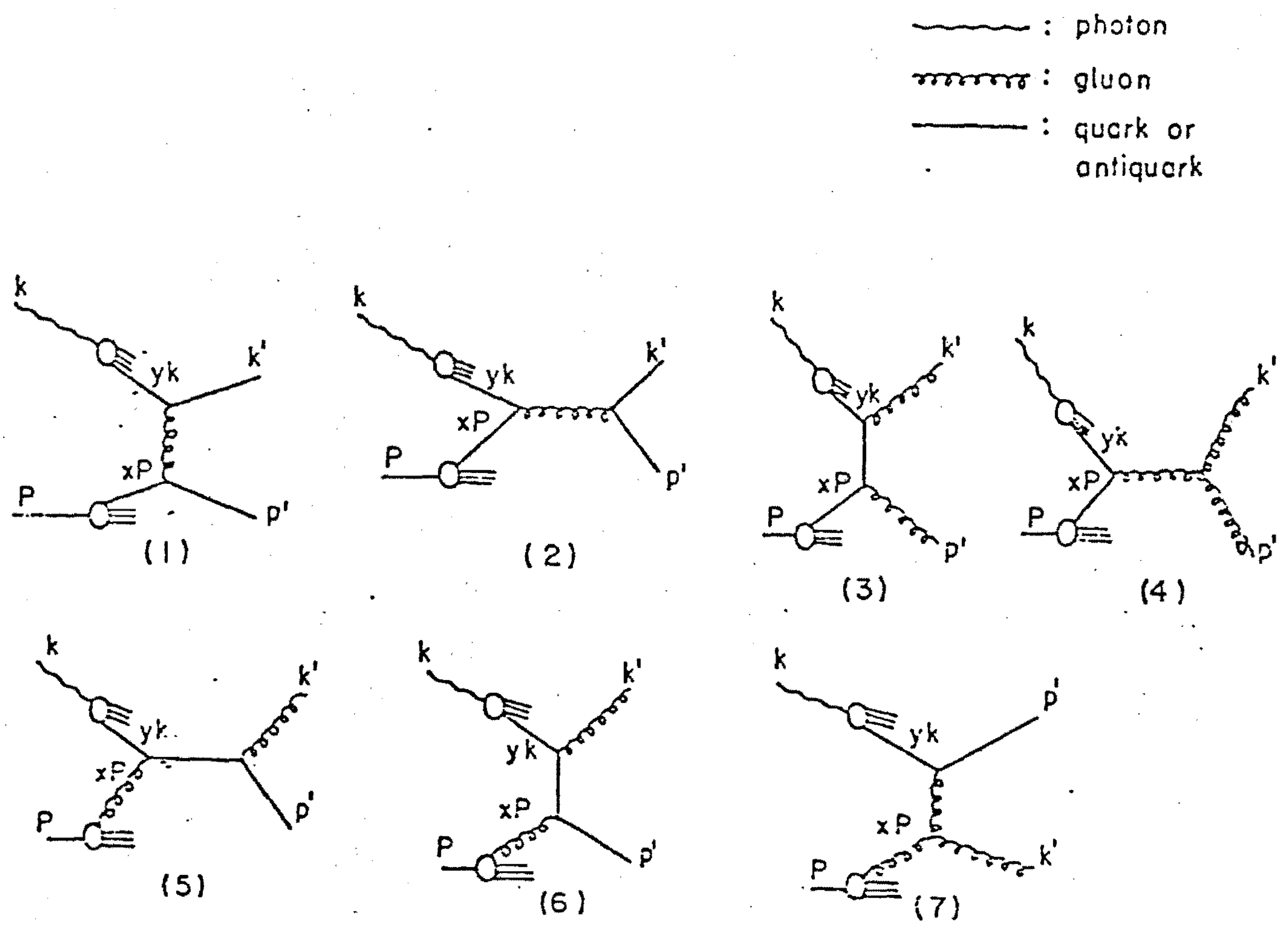

FIG. 3

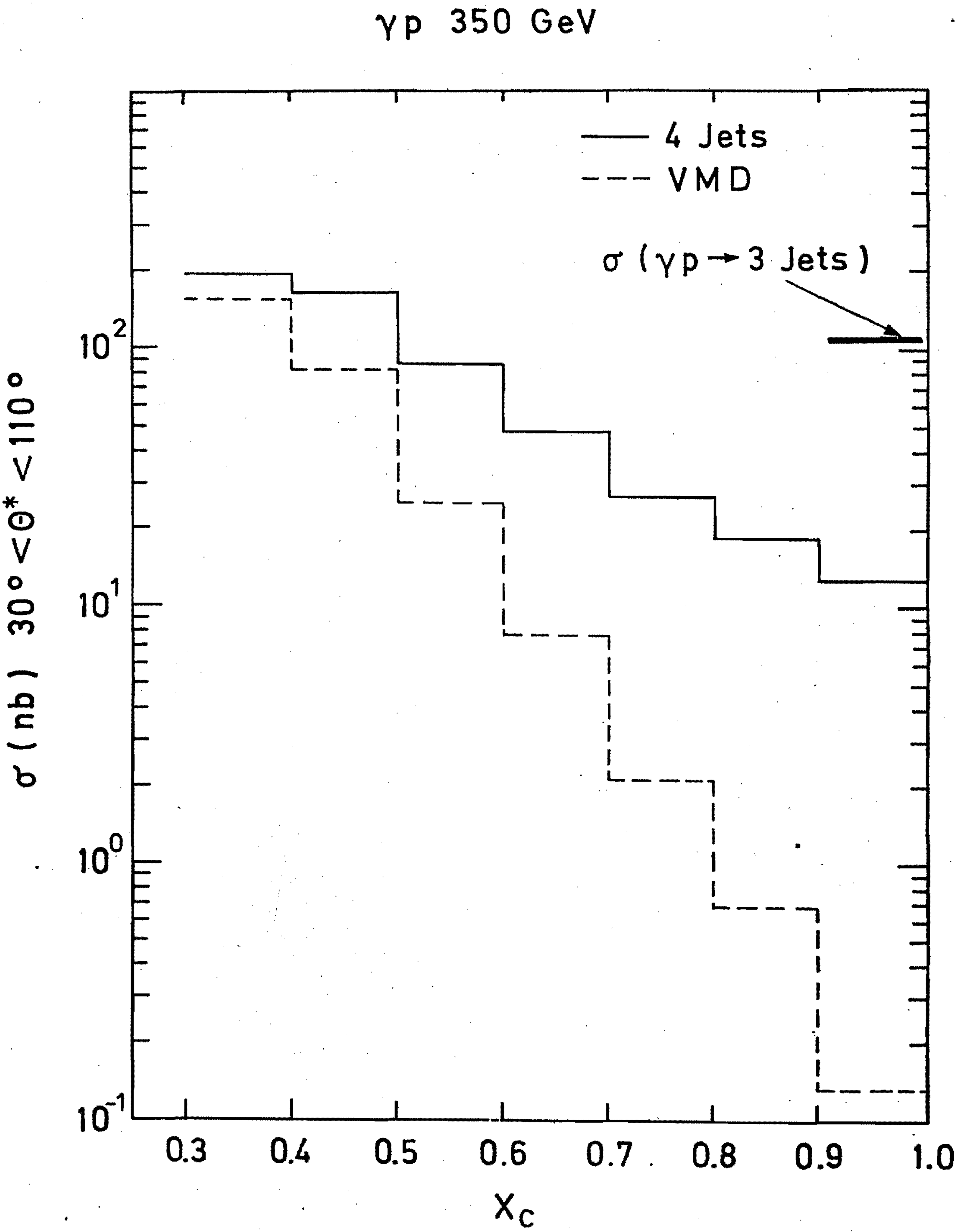

γp 350 GeV
4 Jets
VMD
σ (γp → 3 Jets)
σ (nb) 30° < Θ* < 110°
10^{2}
10^{1}
10^{0}
10^{-1}
0.3
0.4
0.5
0.6
0.7
0.8
0.9
1.0
X_c

Fig. 4

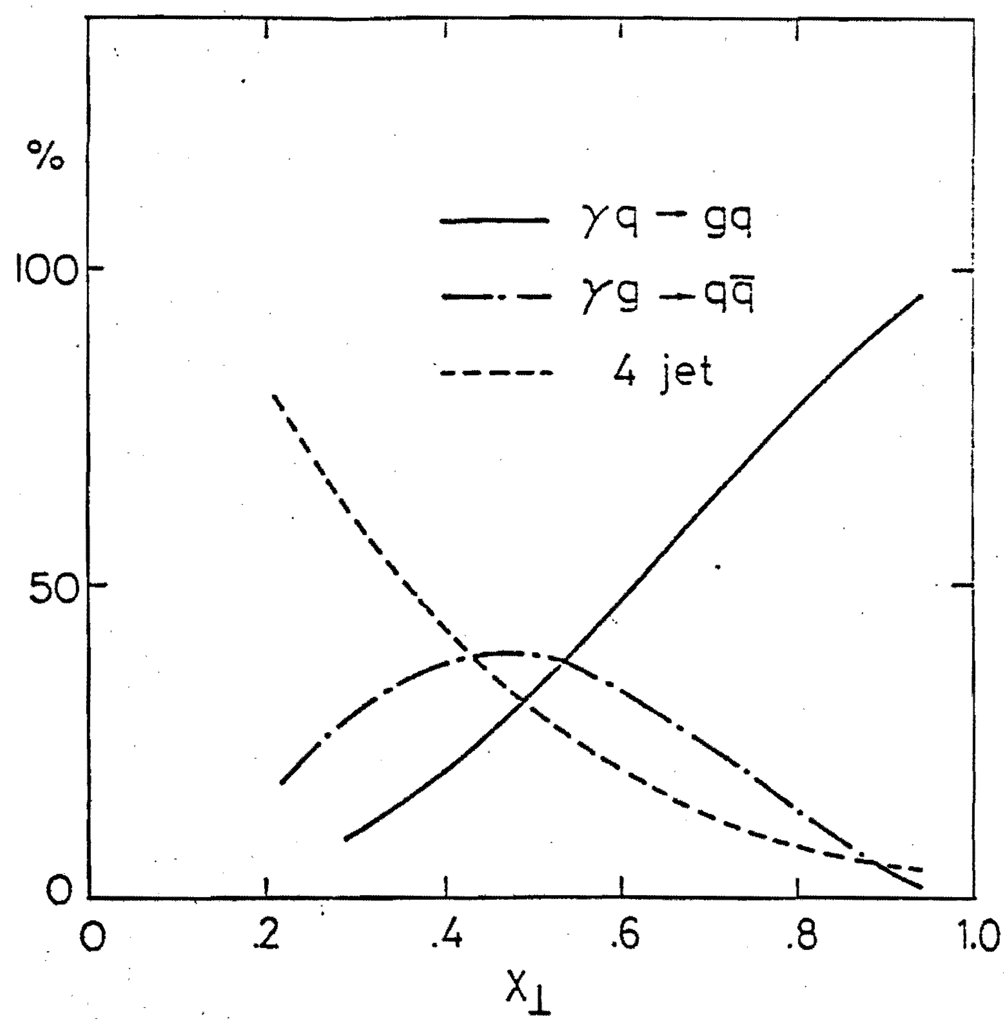

FIG. 5

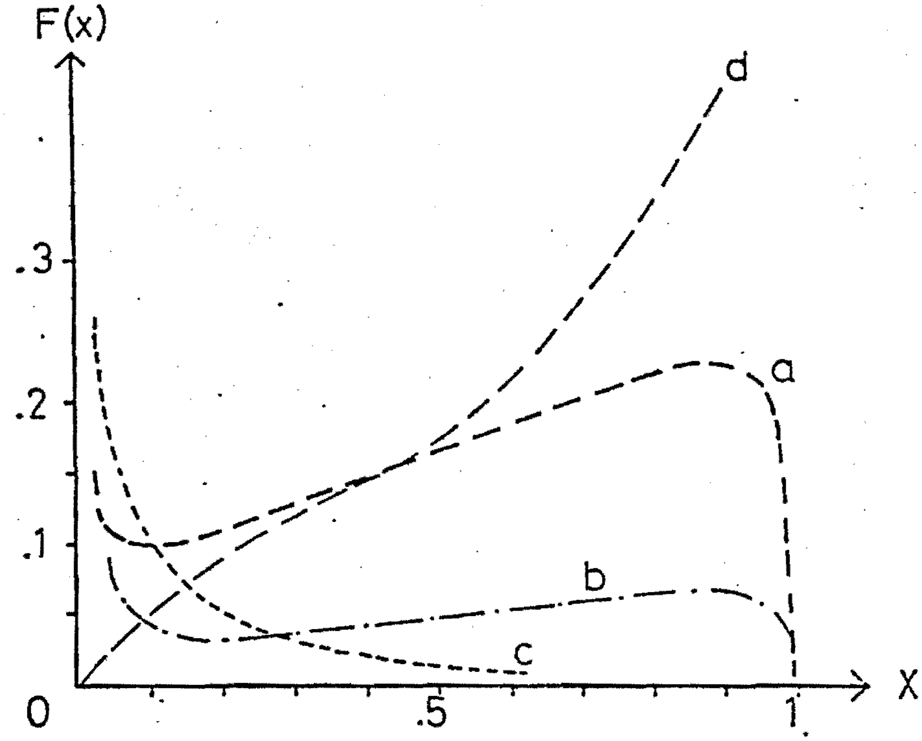

FIG. 6

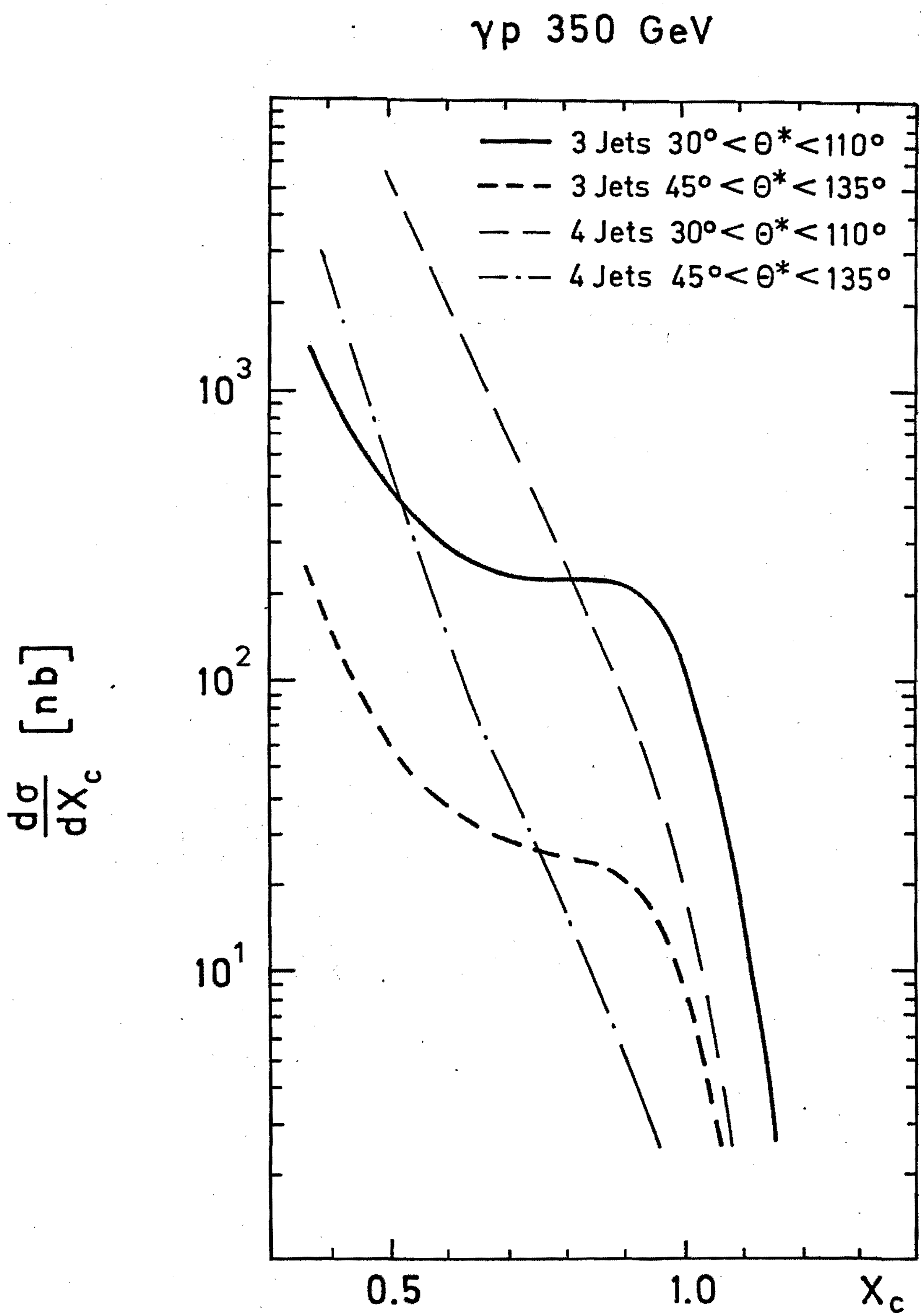
γp 350 GeV
3 Jets 30°<Θ*<110°
3 Jets 45°<Θ*<135°
4 Jets 30°<Θ*<110°
4 Jets 45°<Θ*<135°
10³
10²
10¹
dσ/dX_c [nb]
0.5
1.0
X_c

Fig. 7

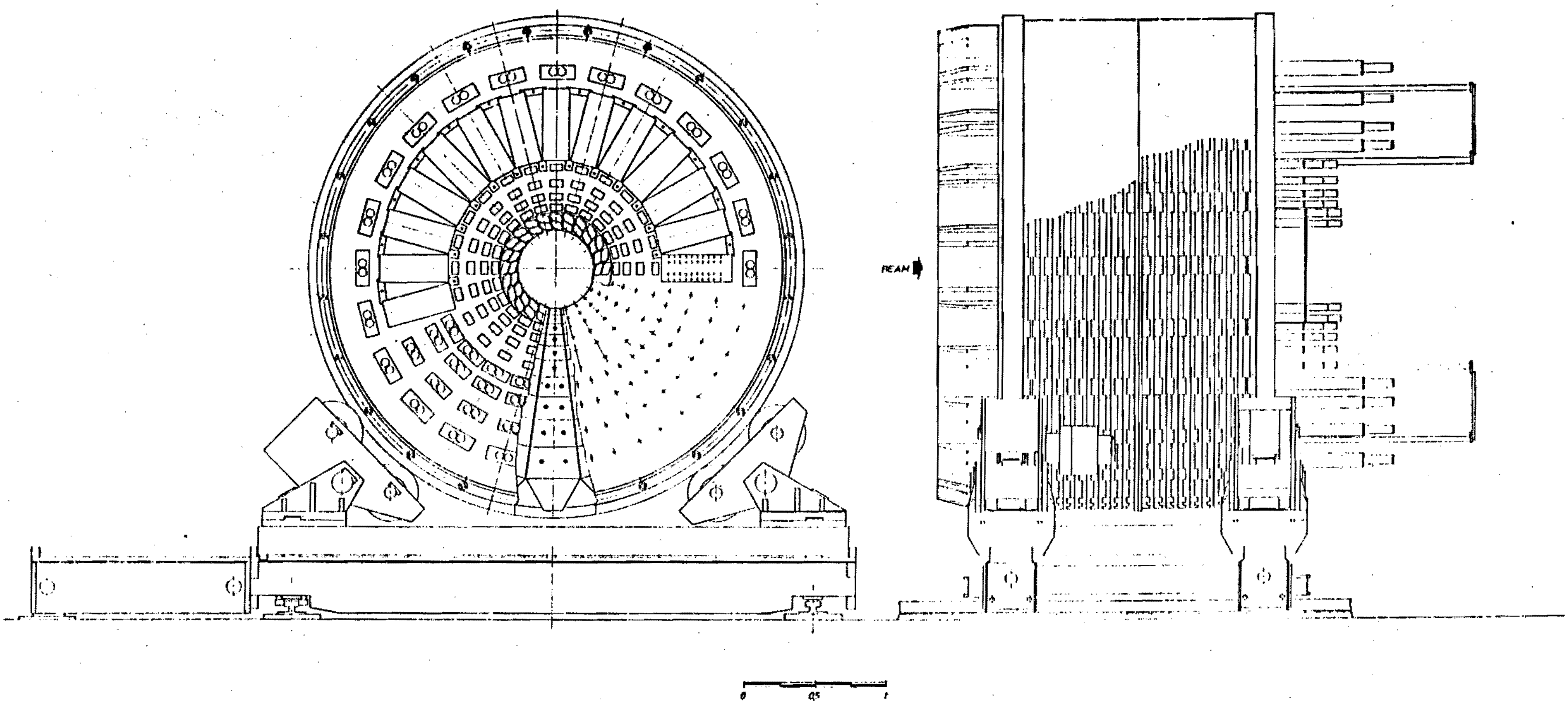

FIG. 8

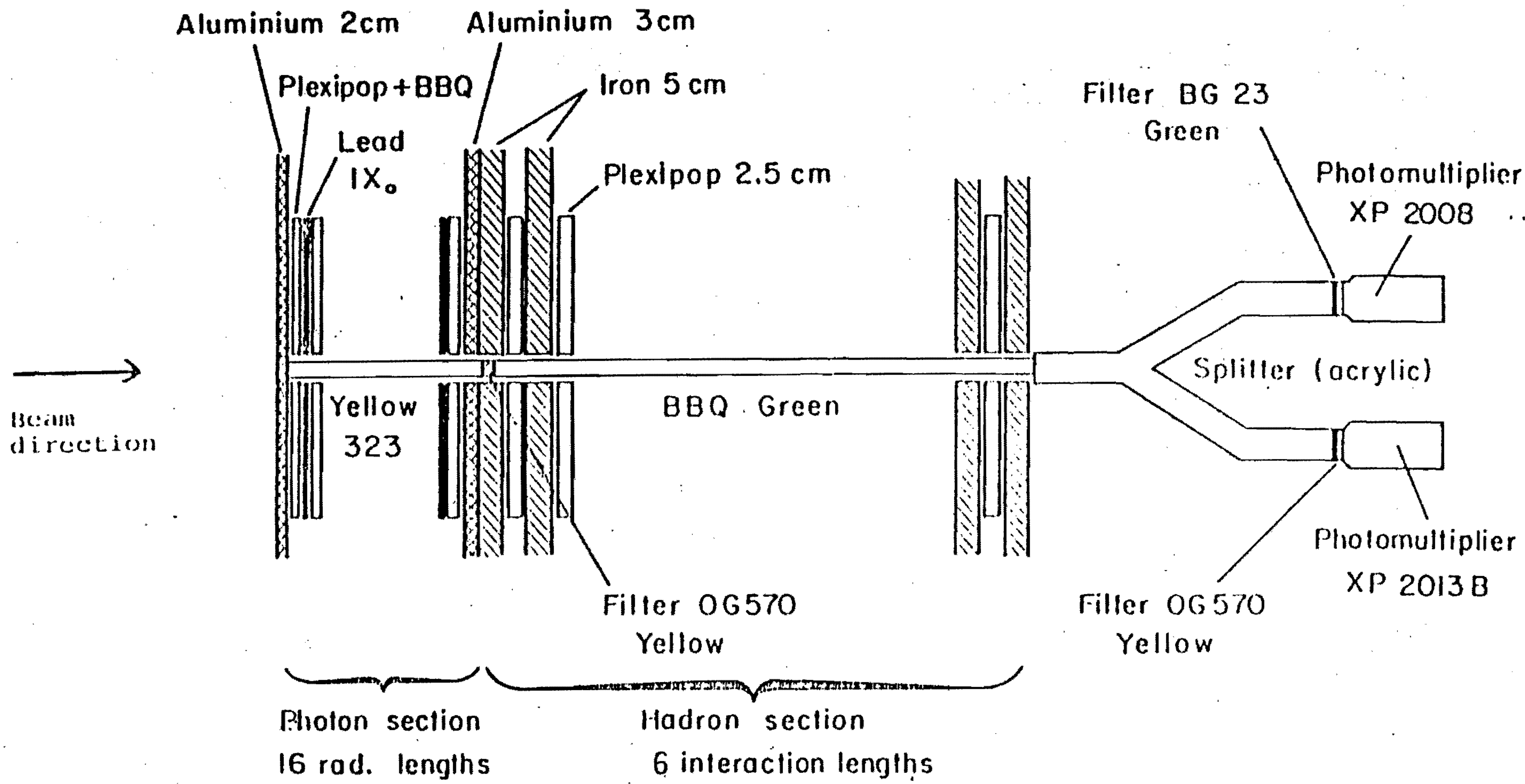
Aluminium 2cm
Plexipop+BBQ
Lead
$1X_o$
Aluminium 3cm
Iron 5 cm
Plexipop 2.5 cm
Filter BG 23
Green
Photomultiplier
XP 2008
Beam
direction
Yellow
323
BBQ Green
Splitter (acrylic)
Photomultiplier
XP 2013 B
Filter OG570
Yellow
Filter OG 570
Yellow
Photon section
16 rad. lengths
Hadron section
6 interaction lengths

FIG. 9

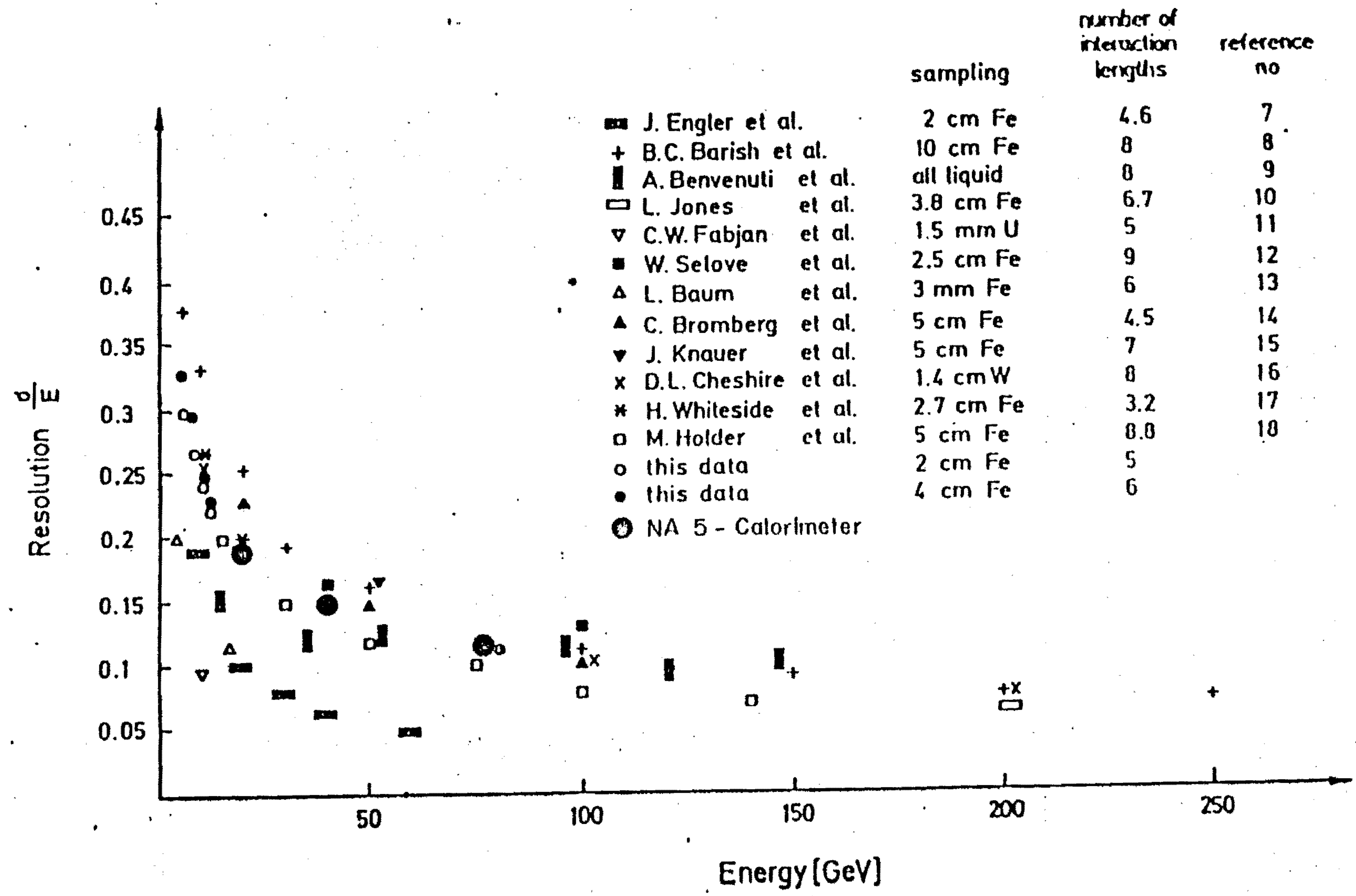

Resolution $\frac{\sigma}{E}$
0.45
0.4
0.35
0.3
0.25
0.2
0.15
0.1
0.05
50
100
150
200
250
Energy [GeV]
sampling
number of interaction lengths
reference no
J. Engler et al. 2 cm Fe 4.6 7
B.C. Barish et al. 10 cm Fe 8 8
A. Benvenuti et al. all liquid 8 9
L. Jones et al. 3.8 cm Fe 6.7 10
C.W. Fabjan et al. 1.5 mm U 5 11
W. Selove et al. 2.5 cm Fe 9 12
L. Baum et al. 3 mm Fe 6 13
C. Bromberg et al. 5 cm Fe 4.5 14
J. Knauer et al. 5 cm Fe 7 15
D.L. Cheshire et al. 1.4 cm W 8 16
H. Whiteside et al. 2.7 cm Fe 3.2 17
M. Holder et al. 5 cm Fe 8.8 18
this data 2 cm Fe 5
this data 4 cm Fe 6
NA 5 - Calorimeter

FIG. 10

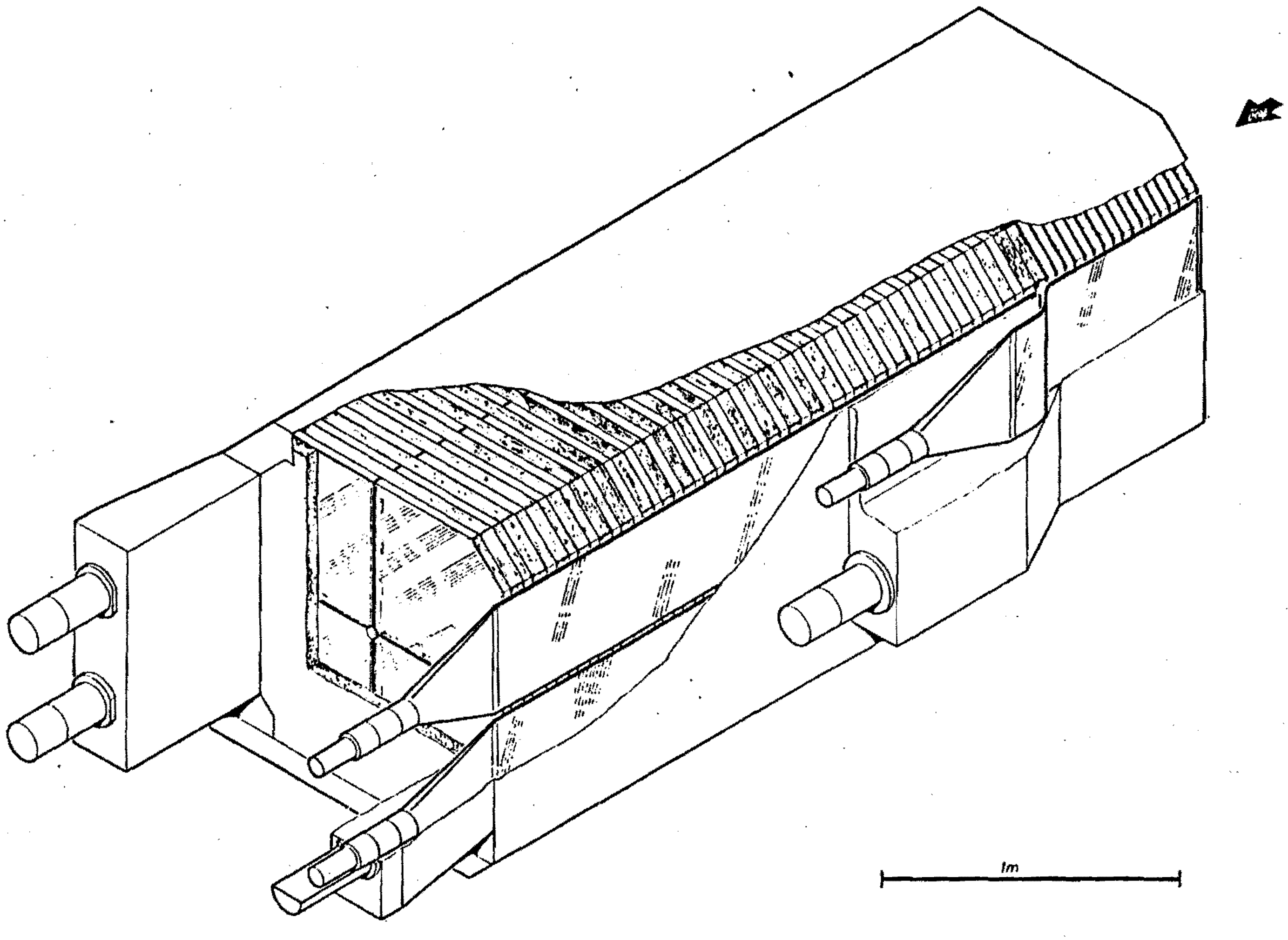

FIG. 11

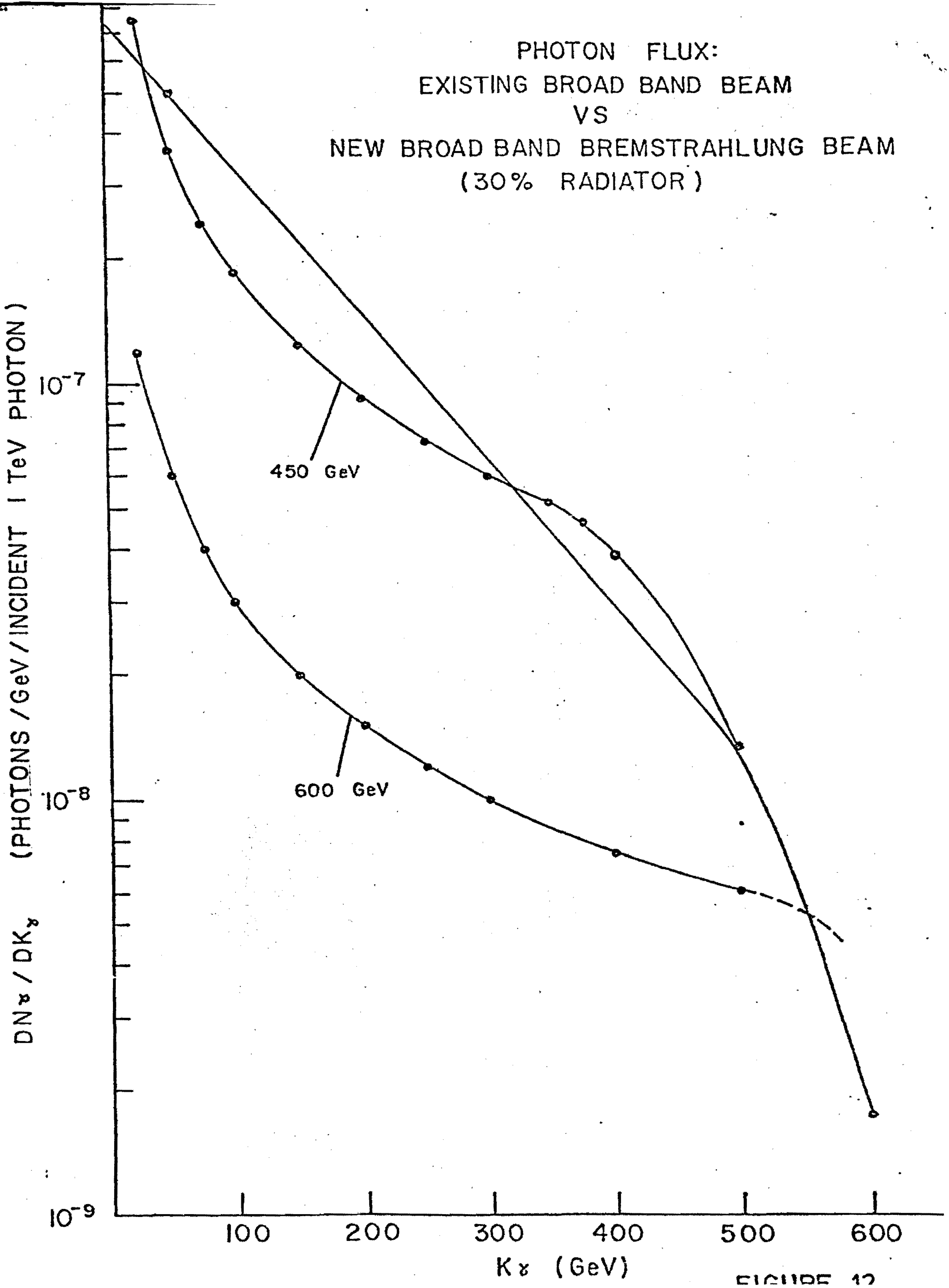
PHOTON FLUX:
EXISTING BROAD BAND BEAM
VS
NEW BROAD BAND BREMSTRAHLUNG BEAM
(30% RADIATOR)
DN_γ / DK_γ (PHOTONS /GeV / INCIDENT 1 TeV PHOTON)
10^{-7}
10^{-8}
10^{-9}
450 GeV
600 GeV
100
200
300
400
500
600
K_γ (GeV)

FIGURE 12